The International Journal of **Medical Robotics** and **Computer Assisted Surgery**

THE INTERNATIONAL JOURNAL OF MEDICAL ROBOTICS AND COMPUTER ASSISTED SURGERY
Int J Med Robotics Comput Assist Surg 2016.
Published online in Wiley Online Library (wileyonlinelibrary.com) **DOI:** 10.1002/rcs.1760

ORIGINAL ARTICLE

An image-guided automated robot for MRI breast biopsy

Kathryn G. Chan[1]
Tim Fielding[2]
Mehran Anvari[3]*

[1]*CSii, Hamilton, Ontario, Canada*

[2]*MDA Robotics, 9445 Airport Road, Brampton, Ontario, L6S 4J3, Canada*

[3]*McMaster University, Department of Surgery, Hamilton, Ontario, L8N 4A6, Canada*

*Correspondence to: Mehran Anvari, McMaster University, Department of Surgery, Centre for Minimal Access Surgery, 50 Charlton Ave E, Hamilton, Ontario, Canada L8N 4A6.
Email: anvari@ijmrcas.com

Accepted: 31 May 2016

Abstract

Background The IGAR (Image-guided Automated Robot) is a robotic platform capable of performing highly accurate clinical interventions under image guidance. The IGAR is unique in that it demonstrates MRI compatibility and maintains safe operation, adequate shielding, high image quality, and accurate robotic control even while in an imaging environment. The IGAR is initially intended for breast biopsy.

Methods Tests for projectile hazards, heating, signal-to-noise ratio loss, and geometric distortion were used to demonstrate MR compatibility. Accuracy and repeatability of the robotic system were tested on benchtop models to establish a baseline of precision.

Results The IGAR averaged an accuracy of 0.34 mm and a repeatability of 0.2 mm. There was no significant distortion attributable to the robot, no projectile risk, and no unacceptable levels of heating.

Conclusion The IGAR system is safe and effective in an MRI environment

Keywords Image guided; automated robot; breast cancer; MRI compatible; needle insertion; biopsy

Introduction

Breast cancer is the second most commonly diagnosed cancer in the world and the most common among women. An estimated 1.67 million new cancer cases were diagnosed in 2012, representing approximately 25% of all cancer cases (1). With such a high incidence rate early detection and diagnosis are crucial components of cancer management. Although mammography is the gold standard for breast screening, Magnetic Resonance Imaging (MRI) is extremely sensitive to cancer in the breast with sensitivity rates pooling around 90% and is therefore indicated in high risk patients (2,3). Breast MRI has resulted in the additional detection of cancers that would otherwise be occult in a mammographic, sonographic, or clinical evaluation (2,4,5). In particular, MRI is indicated for use in evaluations of the contralateral breast (6), and in women with a history of hereditary breast cancer (7–11).

While the sensitivity of MRI adds significant value to diagnostic imaging its specificity is much less reliable and has been reported to range anywhere from 22–50%. Thus, while MRI has superior detection abilities, diagnosis should be

supplemented with a histological analysis of suspicious tissue (2). An MRI-guided biopsy is recommended, as lesions detected on previous MR scans may not be visible or palpable on other image-guided modalities such as stereotactic or ultrasound guided biopsy (12–14). Percutaneous needle biopsy is favourable over surgical biopsy as it is associated with fewer complications and lower cost (15,16).

MRI-guided biopsies have been implemented at multiple clinical centres with great success (17–19). The technique associated with MRI-guided breast biopsy has been described elsewhere (20–23). Liberman *et al*. conducted vacuum-assisted biopsies on lesions that were subsequently excised during surgery and concluded that MRI-guided vacuum-assisted biopsy (VAB) was a quick, accurate, and safe alternative to surgical biopsy (20). In a retrospective review of 85 lesions Orel *et al*. found 9-gauge MRI-guided VAB to be a reasonable alternative to surgery (24).

MRI-guided biopsies provide many benefits but the procedure is technically challenging (25). In similar procedures such as stereotactic breast biopsies lower technical success is associated with radiologists with less experience (26,27). Limited availability of MRI time and equipment has been noted as another major barrier towards adoption (28). The standard practice for MRI-guided breast biopsies involves freehand intervention, with limited mechanisms to ensure coaxial alignment between anesthesia and biopsy tool insertion and no control over the final position of the needle tip. Retargeting of the biopsy tools using an alternate trajectory or multiple insertions is occasionally required if verification imaging reveals inaccurate tool placement, or if additional tissue is required from the target lesion (19). In addition to prolonging the procedure duration, retargeting the biopsy tools may require repeat imaging to verify tool placement and/or multiple anesthesia injections (29,30).

The application of robotic technology to biopsy procedures may significantly increase positional accuracy and operator proficiency. In surgery, robotic systems have demonstrated the ability to perform minimally-invasive procedures, often with accuracy and dexterity that exceeds human limitations (31). These outcomes are translatable and desirable in biopsy, where success of the procedure depends entirely on adequate targeting. Bluvol *et al*. demonstrated that a mechanical arm could be used in biopsy to improve success rates over freehand techniques, reducing needle motion and procedure time for both experienced and naive operators (30). The increased accuracy and repeatability in tool positioning, made possible through robotic technology, could then translate to better patient outcomes.

Several groups are developing robotic technologies for biopsy to address these issues. In one system, a positional device is used for the navigation of a high intensity focused ultrasound (HIFU) transducer under MRI guidance in both the prostate and brain, as this modality provides better contrast than ultrasound (32,33). ROBITOM is a robotic system designed for combined diagnosis, biopsy, and therapy in the isocenter of an MR magnet (34). Larson *et al*. and Tsekos *et al*. developed a probe insertion apparatus integrated with a breast compression device (35,36). Kokes *et al*. designed a hydraulic needle driver for RFA ablation of breast tumors under continuous MRI (37). These systems are still in the prototype stage of development and are far from commercialization.

We have developed an MRI-guided robotic manipulator for needle-based interventions in breast tissue. Unlike other robotic platforms built primarily for research this system is intended for commercialization and is designed for an accelerated product launch. The technology operates in a unique clinical environment and thus its preclinical testing must investigate aspects of MR compatibility, shielding, accuracy, and repeatability. The prototype technology has three main objectives:

1. All new technology must be safe in the MRI environment so that it does not introduce any new risks such as projectile hazards, heating, and vibration.
2. The presence of the robotic manipulator and all associated components must not affect image quality to an extent that would impact targeting accuracy and visualization.
3. The robotic system must retain normal operation and full control during MR imaging.

Materials and Method

System overview

The IGAR (Imaged Guided Automated Robot) is a robotic manipulator initially intended for MRI-guided breast biopsy procedures: IGAR-Breast. It consists of three subsystems: the manipulator, a toolset, and a patient support. An illustration of this system is provided in Figure 1, and the manipulator and patient support are presented in Figure 2. The IGAR has future possible applications in other solid organ biopsies as well as utilization with other imaging modalities.

The IGAR can accurately place tools at a position and along a trajectory specified by a physician. Most system components are within the MR suite, but these are constantly communicating with a control workstation via an Ethernet cable passed through a waveguide into the adjacent room. The IGAR manipulator is commanded using either a bedside pendant in the MR suite or a workstation

DOI: 10.1002/rcs

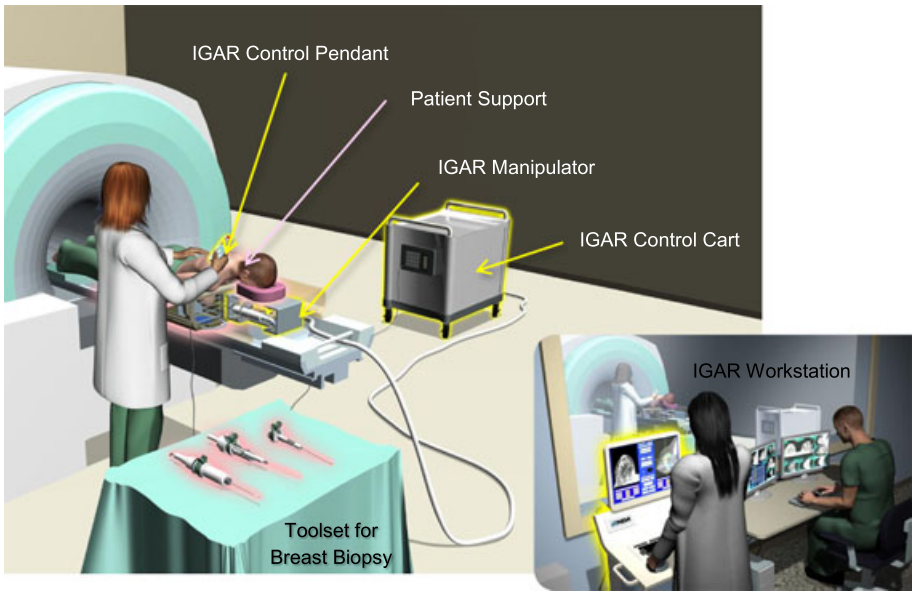

Figure 1. Clinical workspace configuration for the IGAR-Breast system in the MR suite and control room

Figure 2. IGAR-Breast in the modified patient support on top of an MR scanning bed. An anesthesia needle is mounted in a custom tool adapter attached to the manipulator

interface on a laptop in the MR control room. The IGAR's power supply, motion controller, motor amplifiers, and safety circuits are contained within an RF shielded enclosure in a control cart that is kept at the back of the MRI room, minimizing the risk that the RF field will affect electrical components.

Tools can be attached to a mounting arm that runs along an insertion track that is driven by piezoelectric motors. The alignment of the insertion track is achieved through the action of linear and rotary drive assemblies contained within the manipulator casing. These assemblies consist of both pivot and slideable connections. Translation that is applied evenly across the insertion track results in linear movement, while differential motion between the front and back of the insertion track results in horizontal angular motion (yaw) and vertical angle (pitch). Together with rotation these movements give the IGAR 6 degrees of freedom.

For its initial application in breast biopsy, the IGAR uses a set of off-the-shelf biopsy tools including an 18 G anesthesia needle (G01816, Cook Medical, Bloomington, USA), a 10 cc syringe (SS-10S, Terumo Medical Products, Tokyo, Japan), an ATEC Introducer Localization System

DOI: 10.1002/rcs

kit (ILS 0914-20, Hologic, Marlborough, USA), and an ATEC vacuum-assisted biopsy (VAB) handpiece (0914-20MR, Hologic, Marlborough, USA). These tools have been independently evaluated as part of their medical device licensing and are appropriate for use in the MR suite. A custom IGAR adapter exists for each tool. These tool-adapter assemblies are mounted onto the IGAR's end effector arm where they are secured for their use in the clinical procedure. A coupling gear between the mounting arm and the tool adapter allows for rotational movement. This can be used to spin tools directly or to actuate a tool function, e.g. pushing a plunger on a syringe. After the user has indicated which tool is mounted, the IGAR-Breast will automatically adjust the planned insertion accounting for the selected tool's length. Additional parts, including a needle guide and cannula holder, are used to support tools in a fixed alignment.

The patient support structure is a Vanguard Breast MR Table (E8801W, GE Healthcare, Little Chalfont, UK) that has been modified to accommodate IGAR under the headrest. Compression is applied in a super-inferior direction through rear compression plates that are moved forward by the radiology technician and locked into place. A series of fiducial markers is installed into a docking tray that slides under the patient support table, resting under the breast imaging volume. RF coils snap into the medial and lateral sides of the patient support table as per the standard procedure.

The planning interface of the software is presented in Figure 3. The quality of registration is indicated on the right panel. Users are able to scroll through the patient's DICOM images and drop a target at the site of the suspicious lesion. Potential interference with the grid or sides of the patient support are calculated. If necessary, the system will prompt the user to select a different target or approach in order to prevent collisions.

If at any time the software detects an error or an unsafe state, or if the E-Stop (emergency stop) is triggered by the user, the system enters into a 'fail safe' mode. Under these circumstances, power is cut to the motor amplifiers in the IGAR manipulator and brakes are applied to the insertion drive. These brakes are sufficient to prevent any additional movement from the system, but still allow for an operator to manually act against this force to remove tools from a patient if necessary.

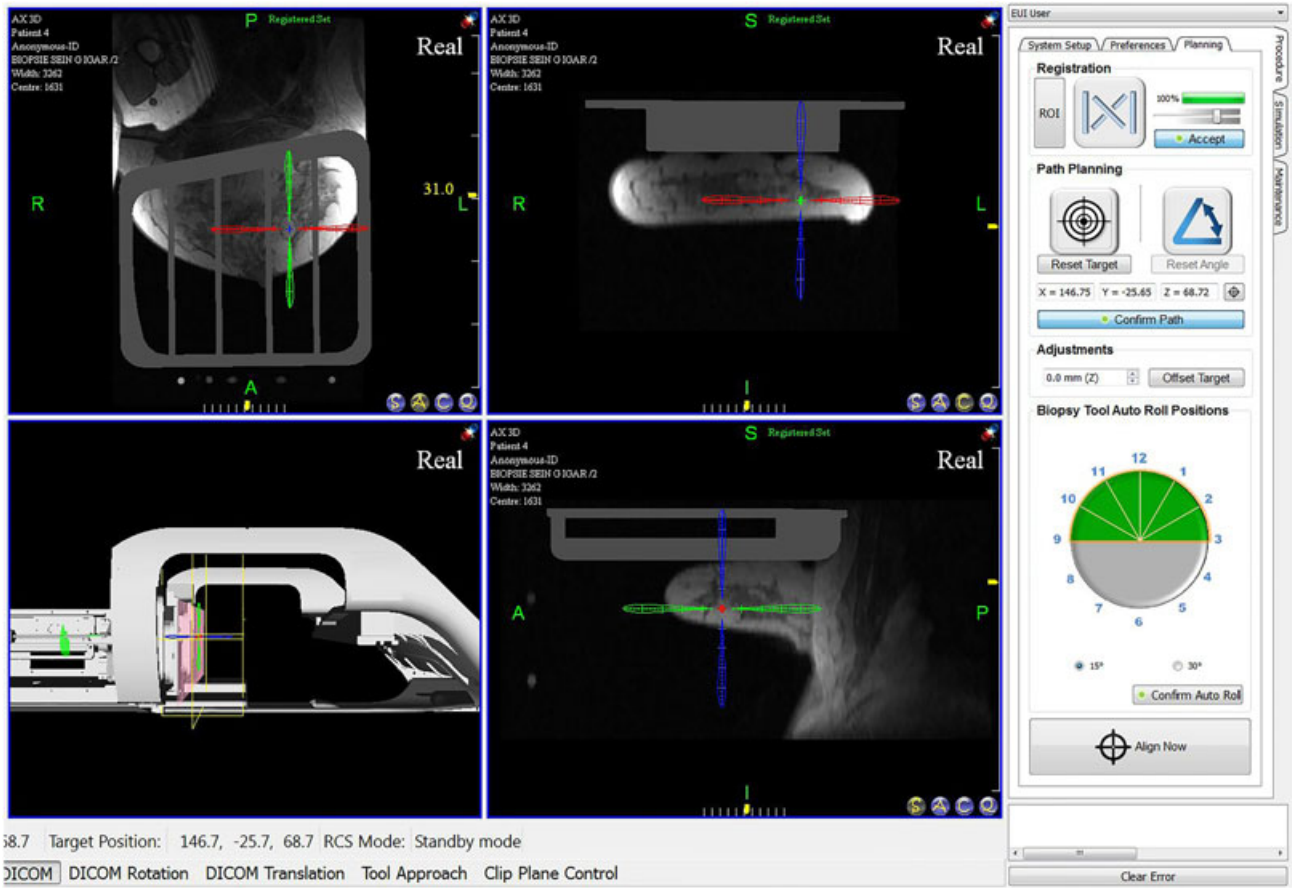

Figure 3. IGAR software interface for target selection

DOI: 10.1002/rcs

In the current model medical interventions are performed outside of the MRI bore in between image scans. At the beginning of the procedure, IGAR components are connected and set up in the MR suite, and the patient is secured. Registration and targeting images are acquired while the IGAR is in the MR bore powered on but in standby mode. For any actual needle insertion, the patient support table is first wheeled out of the MR bore and then the procedure is performed. This workflow was established after image testing on commercially available biopsy tools revealed large artifacts several millimeters in size (Figure 4). If scanned, these artifacts would obscure the lesion of interest, making targeting unreliable. Additionally, interventions performed outside of the MR bore are under the direct visual supervision of the radiologist, which is an additional safety precaution appropriate for this stage of clinical implementation.

Material selection

Regarding MR compatibility, the IGAR manipulator is designed without the use of ferrous material. Reliance on conductive materials is also kept to a minimum to avoid heating and vibration associated with currents generated by switching gradients during imaging. These choices help to preserve the functional performance of the IGAR during image sequencing.

Low susceptibility materials are used near the imaging volume to reduce image distortions. Most of the structural elements of the IGAR manipulator, including the housing and brackets, are made of plastics. Ceramic materials are used in the actuator strips for the piezoelectric motions (Models: HR-N-1, HR-N-8 Nanomotion, Yokne'am Illit, Israel) in an implementation similar to that previously presented in the literature (38,39). The motor housing is susceptible to eddy currents due to its cast zinc alloy material composition. These small vibrations may result in a reduction in actuator force capacity, which was accounted for in the force margin calculations of the IGAR manipulator build. All wiring is copper and routed to prevent loops of significant dimension, and mechanical connections are made from brass or non-magnetic stainless steel.

Instructions specify that the control cart should be placed in the MR suite but outside of the 50 Gauss line. At this distance, the cart is less susceptible to switching gradient fields, so there are fewer restrictions on the use of conductive materials or current loops within the shielded RF enclosure of the cart. Small amounts of ferrous materials can be used without experiencing an attractive force with the magnet.

An existing Vanguard table, already used for MR breast biopsy procedures, is the basis of the patient support. Modifications to the table to accommodate the robotic manipulator and the docking tray were made in consultation with the original manufacturers to mitigate issues relating to patient safety or MR compatibility. The patient padding and RF coils are both commercially available products designed for use with the Vanguard system. The breast restraints that are used to apply compression are also MR compatible; both the front and back breast restraints are composed of PC-ISO. Fiducial markers consist of a series of clear plastic tubes filled with an MR-lucent manganese chloride ($MnCl_2$) solution. These specific materials were selected considering MR compatibility.

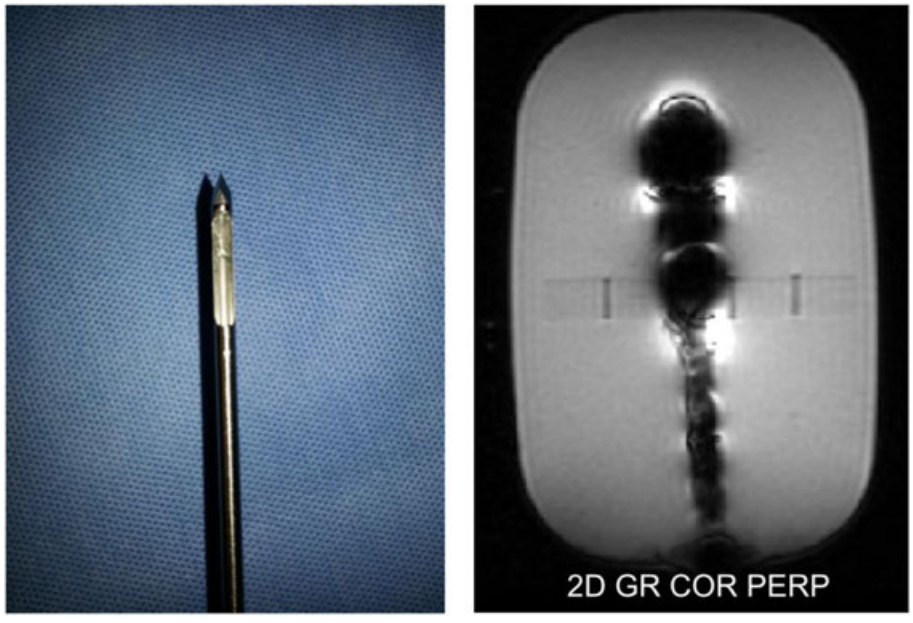

Figure 4. Left: standard VAB needle tip. Right: image artifacts on a needle tip during MR imaging

DOI: 10.1002/rcs

Experiments

Safety and shielding

The static, RF, and gradient magnetic fields could have several effects on this robotic system that could compromise patient safety. System components may shift as a result of magnetically induced torque and force, potentially decreasing the targeting accuracy of this system by skewing image registration. In a worse-case scenario, there is a risk that this movement could cause physical harm or injury to the patient. As such, all IGAR-Breast components intended for use in the MR suite were tested for attractive forces with the magnet. For safe use, the attractive force experienced by the component must remain below 10% of its weight, a criterion chosen to eliminate the risk of a projectile hazard. To measure this effect, each component was suspended from a rope in its location of intended use, and the angle that the component made to the vertical as it became attracted to the magnet's isocenter was recorded. The resultant attractive force was calculated using:

$$F = mg\tan\theta$$

where m is the recorded mass of the component in kg, g is a constant 9.8 N/kg, and θ is the measured angle.

Heating due to RF energy could cause burns and severe discomfort. Induced current and voltages may also contribute to heating, and can affect the integrity of electrical components by causing physical vibrations or electrical overload. A W200 cable connects the IGAR manipulator to the control cart. This cable was evaluated for the risk of cable heating and arcing, as a portion of it lies in the MR bore and on the patient support during image sequencing.

Conservative imaging sequences with high RF energy were run in a 3.0 T GE Discover MR750 scanner in an attempt to induce voltages and currents that could produce cable heating and arcing. Tests were conducted in two environments: a nominal scenario representative of the intended procedure, and a conservative scenario where an excessive amount of extra cable was left on the support table. Four optical temperature sensors were attached to the W200 cable, which was carefully observed for instances of arcing during testing.

In a separate heating experiment, temperature sensors were attached to the medial and lateral RF coils in a 1.5 T GE HDXT scanner. An image sequence was run for 2 hours and temperature fluctuations on the coils were recorded.

Image distortion

The introduction of IGAR-Breast technology in the MR environment could produce image artifacts and may have indirect effects on patient safety if a distorted image is used to guide an interventional procedure. Image artifacts are influenced by a variety of factors including material selection, orientation, and sequencing parameters (40). Geometric distortion of the image may occur due to magnetic field inhomogeneities, which may be the result of position within the magnetic field or may be induced by the susceptibility of an object to produce its own magnetic field. RF field inhomogeneities may contribute to signal nonuniformity. Aliasing artifacts may occur as a result of a poorly selected field of view or phase encoding direction. Metallic objects and magnetic materials used in the construction of IGAR-Breast can produce a variety of artifacts including local distortion and signal loss (41).

Tests were conducted to evaluate the effects of IGAR-Breast components on image quality. Imaging sequence parameters were chosen with input from hospital staff to mimic a standard breast biopsy procedure. Testing was conducted on both a 1.5 T GE HDXT scanner and in a 3.0 T GE Discovery MR750, as the IGAR-Breast is indicated for use in both imaging environments. A 3D Gradient Echo (TR = 7.46 ms, TE = 4.2 ms, flip angle = 10°, bandwidth = 62.5 kHz, matrix = 256 × 256, FOV = 18.8 cm × 18.8 cm, slice plane = axial, slice thickness = 2.2 mm, acquisition time = 1.58 min) was used in the 1.5 T scanner while a 2D Fast Gradient Echo (TR = 6 ms, TE = 2.11 ms, flip angle = 30°, bandwidth = 62.5 kHz, matrix = 256 × 256, FOV = 24 cm × 24 cm, slice plane = axial, slice thickness = 2.0 mm, acquisition time = 1.12 min) was used in the 3.0 T scanner.

To measure geometric distortion, a box phantom with known dimensions (shown in Figure 5) was filled with a solution of 0.079 mmol/L $MnCl_2$. The same phantom, minus the inner grid, was used again to measure signal-to-noise (SNR) ratios.

Images were acquired in a stepwise fashion as new IGAR components were gradually introduced. The sequence of testing configurations describing the layout of IGAR-Breast components in the MR bore is available in Table 1. For each SNR test, two consecutive scans were acquired with auto-shimming off in between images that would form a pair. In each distortion test, image sequencing was executed with both RL (right-left) and AP (anterior-posterior) frequency encoding, while only RL was used for SNR.

SNR was calculated using two methods: the subtracted slice method and the single slice method, which are detailed in IEC-62461-1 sections 4.2 and A.1.2. Each of these methods has characteristic advantages and disadvantages. The subtracted slice method requires two images, doubling the acquisition time making the results more sensitive to system drift (42). The single slice method is more sensitive to non-uniformity as it depends on a single image (43). SNR should be the highest in the

DOI: 10.1002/rcs

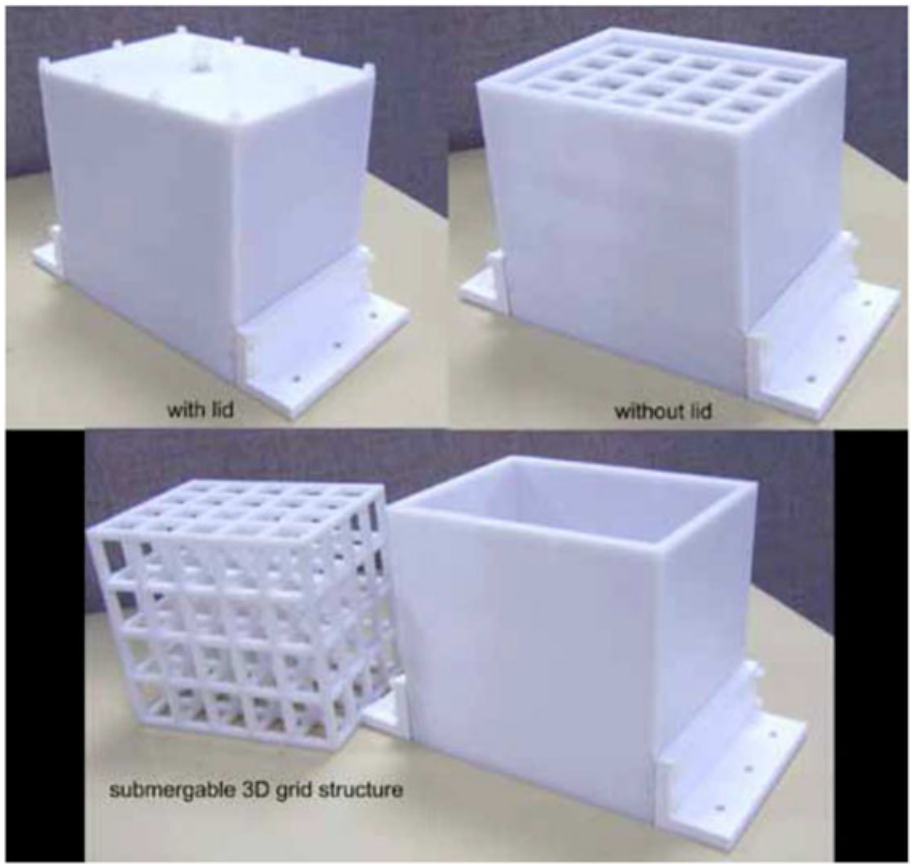

Figure 5. Custom phantom used to measure geometric distortion and signal-to-noise ratio

Table 1. Sequence of test configurations during image quality tests

	1.5 T GE HDXT scanner	3.0 T GE Discovery MR750 scanner
SNR Testing	Baseline (IGAR powered off); IGAR in standby mode	Baseline (IGAR powered off); IGAR in standby mode
Distortion Testing	IGAR in standby mode, with patient support; No IGAR, just patient support	No IGAR, just patient support; Baseline (No IGAR, no patient support); IGAR powered off, no patient support

centre of the imaging volume, between the medial and lateral coils. However, since the IGAR-Breast employs superior-inferior compression, the breast tissue is pushed up to the superior edge of the patient support and is in line with the superior edge of the coil. As a result the tissue volume ends near the middle of the image volume. During testing, the phantom was positioned in this arrangement to represent the clinical scenario. Consequently, two imaging regions were evaluated for SNR: a superior slice where the coil is expected to be less sensitive and an inferior slice where the coil is expected to be most sensitive.

Distortion was evaluated by comparing the known physical dimensions of the phantom grid with the measured grid dimensions on the acquired MR scans. Once again, superior image slices are expected to have the worst results, due this time to the proximity to IGAR electronics under the headrest that could cause image distortion.

Accuracy and repeatability

An automated robotic system with high positional accuracy could eliminate dependence on human calculations and dexterity for tool placement, and potentially overcome the targeting limitations of a fully manual biopsy procedure. Positional accuracy is defined as the difference between the commanded position of the tool tip and the

DOI: 10.1002/rcs

actual position of the tool tip as measured by an optical tracker (Polaris Optical Tracking System, NDI Medical, Waterloo, Canada). During the test procedure, a rigid test tool was driven to 34 target positions in free space across IGAR's workspace using both straight and angled approaches. Following an initial test run, the IGAR kinematic model was corrected to more closely match the measured optical tracker positions by applying a rigid body transform, comprising of a rotation matrix R and translation vector T calculated through a Procrustes analysis of the 34 point pairs. The total error measured in the post-calibration system is the best representation of the errors attributable to IGAR performance.

$$p_{corrected} = Rp + T$$

Repeatability is defined as the deviation in actual tool tip position between subsequent insertions to the same point. IGAR was used to drive to each of the 34 target positions twice, and repeatability was averaged over the workspace. Two IGAR systems, models 201 and 202, were used to assess accuracy and repeatability.

Results

Safety and shielding

The tool adapters (for the anesthesia needle, trocar, and VAB handpiece), connecting cables, bedside pendant, and IGAR manipulator were evaluated for their attractive forces. With the exception of the pendant, each component was suspended approximately half a metre from the opening of the MR bore, as this is the approximate location where the tools will be installed for the procedure. None of the components experienced any attractive forces. The pendant was tested further from the bore opening in a position representative of where the radiologist would typically stand. At this location, the pendant did not experience significant attractive forces. The pendant does contain a metallic spring that can be attracted to the magnet if held close enough, but this force is not sufficiently significant to pose a safety hazard.

The control cart could not be evaluated using the suspension method. Instead, the control cart was gradually introduced into the MR suite while held back using a rope secured to a handheld force gauge. The force required to move the control cart backwards from rest was recorded at different stages, each time moving closer towards the magnet. No attractive forces were measured half a metre from the MR bore. As an extra precaution, instructions for use specify that the control cart should be set up at the back of the MR suite behind the 50 Gauss line. These results demonstrate that IGAR components are safe to introduce to the clinical environment. Tool adapters and accessories can be incorporated into the standard workflow without any additional precautions.

Although the biopsy tool adapter experienced no attractive forces, the adapter-tool assembly experienced more than 19 N of force when suspended half a metre from the MR bore. This reinforces the idea that off-the-shelf tools cannot be safely used within the MR magnet, and that all interventions should take place after the patient has been wheeled out of the bore, which is consistent with standard clinical procedure.

With the manipulator in a nominal position, no cable heating was recorded. In the conservative position, a maximum temperature rise from 20 °C to 38 °C was observed from four optical temperature sensors over 6 minutes, as presented in Figure 6. The final temperature was still below touch temperatures and within IEC 60601-1 standards, which list a maximum temperature of 43 °C for parts in contact with patients for longer than 10 minutes. Based on these results, the IGAR cable was determined to be suitable for use. To reduce the possibility of any remaining risk, the IGAR-Breast instructions for use include diagrams and statements describing proper cable routing and warning about the risk of moderate cable heating if too much cable is routed through the bore. Additionally, the cable attaches to the manipulator under the patient headrest and is routed out of the bore away from the patient. In this workspace configuration it should

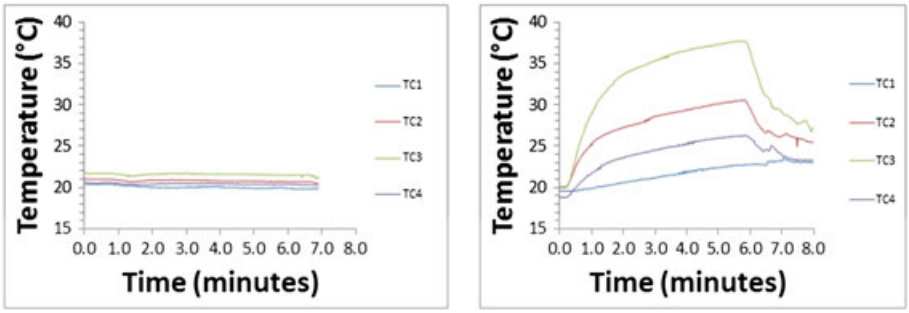

Figure 6. Results from cable heating tests in a nominal position (left) and a conservative position (right)

DOI: 10.1002/rcs

not be possible for the patient to come in contact with the cable. These procedural cautions coupled with the physical protection provided by the shielded cables ensure safe operation.

In the case of coil heating, the magnet temperature gradually rose during the imaging sequence. Approximately 45 minutes into the scan, the internal temperature exceeded the safety limits of the GE system, and cooling fans were engaged. This temperature rise was the result of the continuous imaging sequence, and is not attributable to the IGAR-Breast hardware. The temperature probes on the coils measured less than 1 °C rise over the 45 minutes during which scanning was active. The IGAR-Breast system does not appear to influence the coil system or cause any unexpected heating, again demonstrating effective shielding and MR safety.

Image distortion

SNR results are available in Table 2, and corresponding image scans for the 1.5 T scanner are presented in Figure 7. SNR values were lower for the single slice method compared with the double slice method. This can be attributed to the non-uniformity of noise in the images from ghosting and artifacts, which increases measured noise levels and decreases SNR.

SNR image scans from the 3.0 T scanner are presented in Figure 8. Baseline SNR at the 3.0 T scanner was approximately 25% lower than baseline SNR at the 1.5 T scanner. This could be the result of multiple environmental factors. Commercially available diagnostic breast coils were used in the 1.5 T scanner, while research coils were used in the 3.0 T scanner. The research coil contralateral to the imaging volume containing the phantom could not be turned off, and may have introduced additional noise in the 3.0 T environment. Baseline ambient noise might also have differed between the two facilities. The scanning parameters differed slightly on each magnet; in particular the use of thinner slices, larger FOV, and a shorter TR with the 3.0 T scanner may have contributed to the lower SNR.

The IGAR-Breast workflow would require the IGAR manipulator to be present but in standby during image acquisitions. Comparing the baseline SNR measurements with the configuration where the IGAR is in standby indicates the effects of IGAR electronics on SNR measurements. In the 1.5 T scanner, the IGAR manipulator caused SNR to drop by approximately 13%, while only causing a drop of 2.5% in the 3.0 T scanner. This difference may be caused by the relatively high baseline noise in the 3.0 T scanner, such that any additional noise introduced by the IGAR had little net effect. In both cases, the relative drop in SNR as IGAR technology was introduced into the MRI environment is lower than the difference in baseline SNR between scanners.

Across both scanner and test configurations, SNR levels at the front of the breast volume in the superior slice were 30–40% lower than SNR levels in an inferior slice. Some variation of SNR results throughout the breast is expected in a standard breast scan due to the distribution of coil elements.

Figure 9 depicts the grid phantom on superior image slices in the 1.5 T scanner. Grid lines should be 21 mm in the RL direction and 24 mm in the in the AP direction. Under all test and scanning configurations, measured dimensions were within 0.5 mm of their expected value. However, this should not be taken as a direct indication of error as pixel dimension is 0.73 mm in the DICOM viewer, making precise measurements below this threshold impossible. Therefore, in a 1.5 T scanner the presence of the IGAR manipulator does not distort the image and does not result in any significant image degradation.

Figure 10 depicts the grid phantom on superior image slices in the 3.0 T scanner. Grid lines should again be 21 mm × 24 mm, though in this case pixel dimension is 0.94 mm. In the baseline image with no patient support or manipulator present, the image distortion reaches a maximum of 0.7 mm, attributable to pixelation. With just the IGAR present (bottom row of Figure 10) distortions are within 0.4 mm, suggesting that the manipulator does not cause image distortion. In the clinical scenario with both the IGAR and the patient support present, distortion reaches a maximum of 2.4 mm in the AP frequency encoding direction, and 2.0 mm in the RL frequency encoding direction. These errors can be traced back to the patient support, as the IGAR was previously exonerated from this magnitude of error.

Table 2. Signal-to-noise ratios in both the 1.5 T and 3.0 T scanner from two calculation methods

		Subtraction Method		Single Image Method	
Configuration		**Inferior Slice**	**Superior Slice**	**Inferior Slice**	**Superior Slice**
1.5 T GE HDXT	Baseline (IGAR powered off)	56.6	40.0	43.1	25.0
	IGAR in standby mode	49.0	30.5	39.3	23.1
3.0 T GE HDXT	Baseline (IGAR powered off)	41.8	28.9	32.7	19.9
	IGAR in standby mode	45.3	25.0	32.0	19.3

DOI: 10.1002/rcs

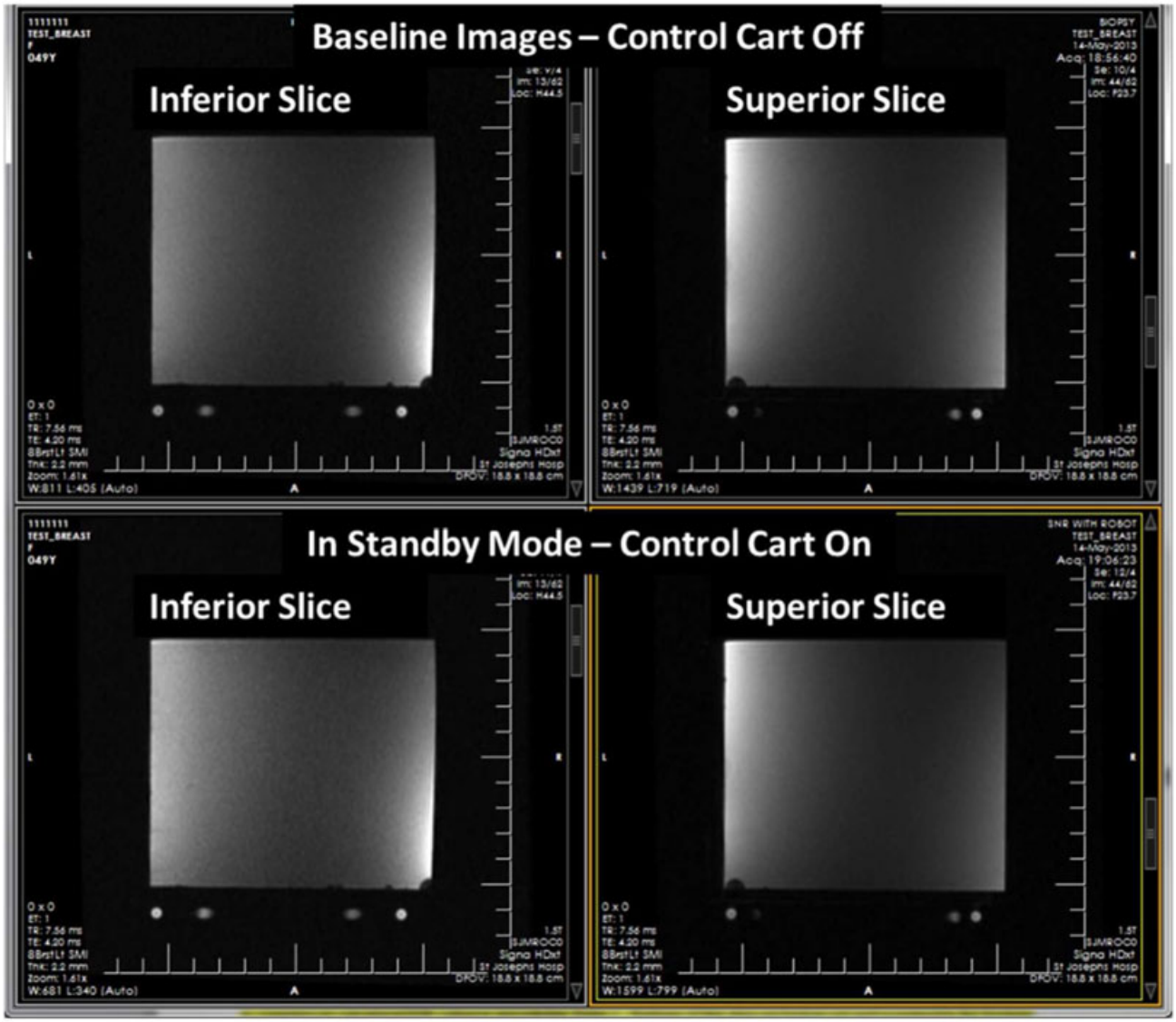

Figure 7. SNR test results from a custom phantom in the 1.5 T scanner. White represents areas of high signal and black represents areas of low signal. No discernable difference is appreciated when the control cart is powered on. Signal is noticeably stronger in the inferior slices

Accuracy and repeatability

Accuracy test results are presented in Table 3. Following calibration, average accuracy error was recorded as 0.40 mm for system 201 and 0.34 mm for system 202. This demonstrates that the robot has sub-millimeter targeting ability in free space. A heat map of total positional error across all targets in the IGAR workspace is presented in Figure 11.

Repeatability test results are presented in Table 4, and averaged to 0.2 mm for both systems. A heat map of the repeatability across all targets in the IGAR workspace is presented in Figure 12. These sub-millimeter results show that IGAR-Breast will have excellent targeting ability in the context of MRI guided interventions, especially when considering that pixel dimensions on DICOM viewers can be close to 1 mm.

Discussion

These experiments were designed to evaluate the pre-clinical efficacy of the IGAR-Breast system in terms of MRI compatibility, safety, and accuracy. While these results do not assess the operational functionality of the IGAR-Breast in end-to-end testing, they do explore environmental factors that may affect performance. This is a critical stage

DOI: 10.1002/rcs

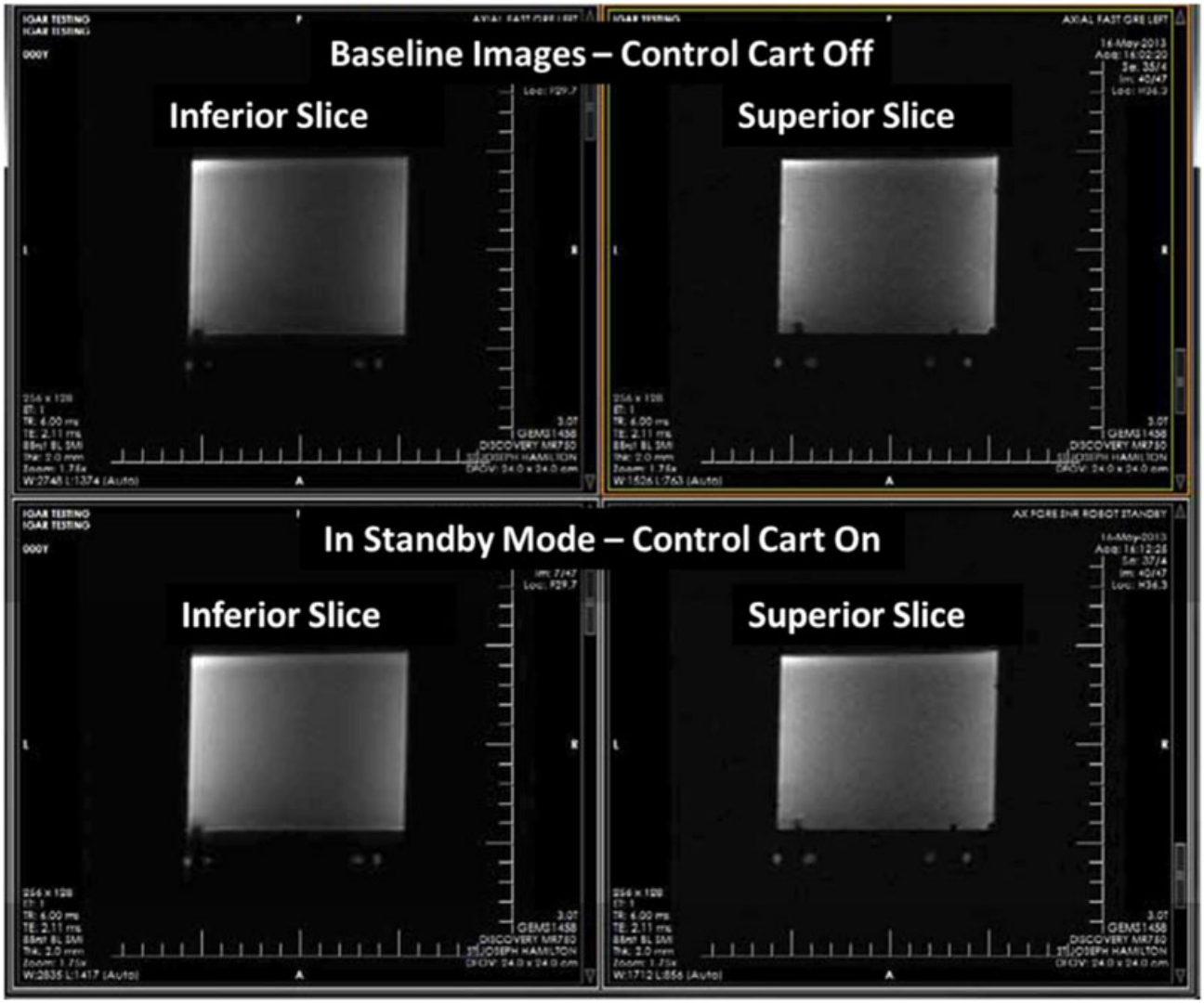

Figure 8. SNR test results from a custom phantom in the 3.0 T scanner. White represents areas of high signal and black represents areas of low signal. No discernable difference is appreciated when the control cart is powered on. Signal is noticeable stronger in the inferior slices

in the design process as it allows us to identify, isolate, and correct potential sources of error. Overall, test results demonstrate that IGAR- Breast technology is appropriate for a clinical environment. Diagnostic quality MRI images with high SNR and minimal distortion can still be obtained while IGAR is operational. Careful material selection, including the use of plastics and ceramics, coupled with RF shielding further prevents MRI image degradation. These design choices also ensure that the technology can function as intended in an MR environment, maintaining the high degree of accuracy and repeatability evidenced by benchtop testing.

The results of the verification of accessories and coil temperature and heating tests demonstrate that the IGAR-Breast does not induce projectile motion, tissue heating, or electronics heating. Vibration of components was not observed in any of the experiments conducted. Design choices in material selection, system layout, and workflow were made to reduce the risk of hazards associated with new technology. The materials used in the IGAR-Breast system shares a similar level of MRI-related safety risk as the standard manual procedure.

The assessment of distortion and SNR produced images with a quality that was adequate but could be improved. Distortion was notable in one testing configuration: in the 3 T scanner at the superior edge of the phantom with both the manipulator and the patient support. Based on these results, metallic fasteners were replaced with brass parts in later iterations of the patient support table. It is expected that this change will further improve image quality. SNR results were consistently better towards the back of the phantom near the middle of the coil. This outcome is a consequence of the compression direction of the

DOI: 10.1002/rcs

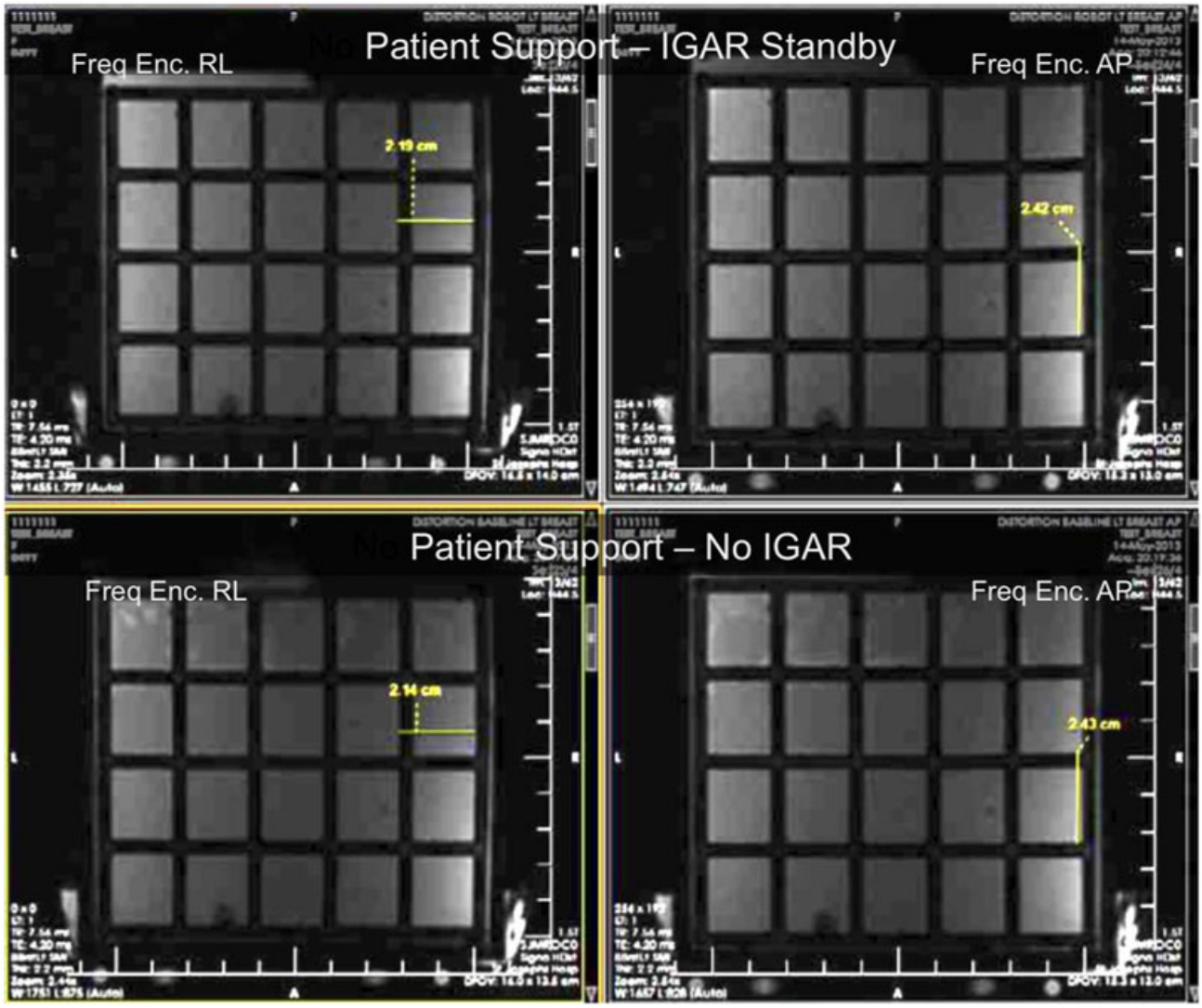

Figure 9. Geometric distortion test results from a custom phantom in the 1.5 T scanner. The imaged phantom appears to be regular with straight edges, matching the construction of the physical phantom in Figure 5

IGAR-Breast and cannot be remedied without redesigning the patient support. While SNR values at the superior edge of the phantom seemed reasonable, it is possible that targeting accuracy may vary as a function of depth of lesion location. Modifications in patient positioning may be able to further improve signal quality, but IGAR technology itself does not cause any significant image distortion.

Accuracy and repeatability testing show sub-millimeter results demonstrating that the IGAR system has superb targeting potential. Although the results would be more representative if testing was conducted in the MRI suite, the NDI Polaris system is not MR-Safe and thus the test procedure would be impossible to execute. However, given the results from the MRI compatibility testing and the conscious choices in material selection there is evidence to suggest that the IGAR's targeting abilities are transferrable to the MRI environment. The IGAR manipulator's performance was informally evaluated throughout MRI testing and product development. The IGAR was routinely commanded to complete certain tasks in order to demonstrate that its benchtop functionality could be reproduced in an MR field. Throughout all testing, the IGAR behaved as expected, suggesting that the IGAR maintains its high degree of accuracy. At times, an E-Stop was automatically and unexpectedly engaged by the system, flagging a potential safety issue. These false E-Stops only occurred during MRI image sequencing and therefore should not impact the proposed clinical study procedure as the IGAR is only commanded to move when the patient is outside of the MR bore after imaging is complete. Users were able to manage the E-Stop triggers

DOI: 10.1002/rcs

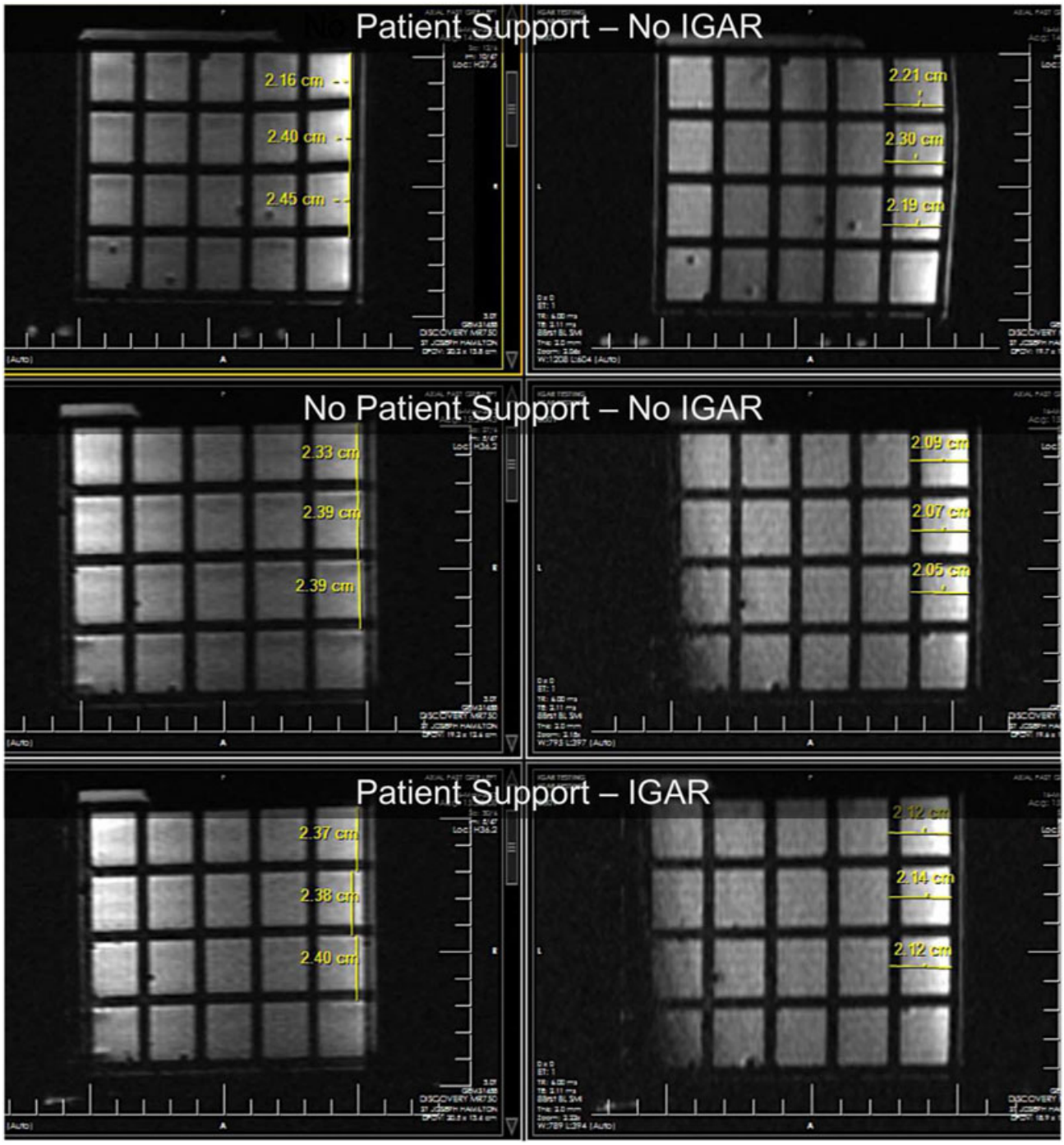

Figure 10. Geometric distortion test results from a custom phantom in the 3.0 T scanner. Upon visual inspection the imaged phantom appears regular, though grid lines are slightly curved in the AP encoding direction (right panel of images).

appropriately, maintaining full system control. These casual observations will be followed by a more rigorous and quantitative assessment of the targeting accuracy of the IGAR, as well as a thorough investigation into the source of the E-Stops.

End-to-end testing in phantom models and results from ongoing clinical trials will provide an opportunity to evaluate the total accuracy of the system. Errors observed in end-to-end testing can be attributable to a number of sources including IGAR free space accuracy, MRI registration accuracy, installation of the robotic manipulator in the docking tray, and installation of tools onto the end effector. Additional sources of error may only be evident at the time of clinical trial. For example, patients may shift

DOI: 10.1002/rcs

Table 3. Positional accuracy of IGAR models 201 and 202 pre and post calibration

	201Pre-Calibration	201Post-Calibration	202Pre-Calibration	202Post-Calibration
Average total error (mm)	1.26	0.40	0.92	0.34
Worst-case total error (mm)	1.45	0.76	1.23	0.64

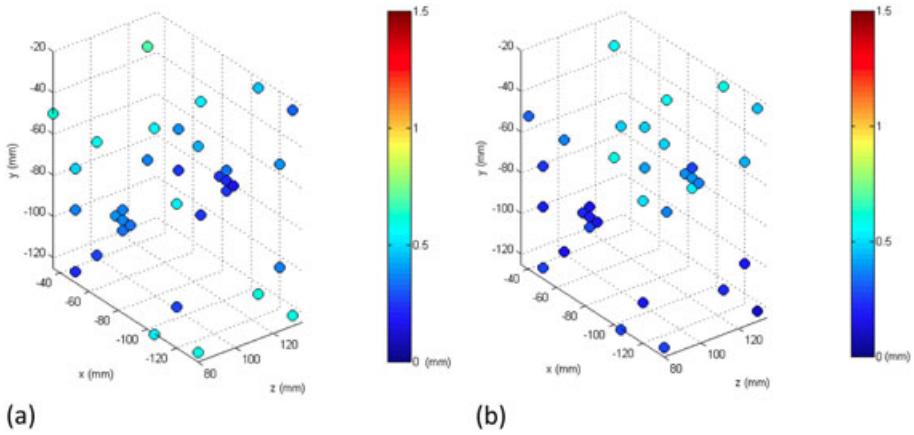

Figure 11. Total errors for all targets in (a) IGAR 201 and (b) IGAR 202 post-calibration

Table 4. Repeatability of IGAR models 201 and 202

	201	202
Average repeatability (mm)	0.20	0.20
Worst-case repeatability (mm)	0.31	0.36

and reposition themselves, moving lesions away from their targeting position or creating motion artifacts that may affect the diagnostic quality of the images.

Figure 13 shows IGAR's software user interface during a procedure in a patient from the clinical trial. The radiologist is able to scroll through the set of MR images and choose a target. The IGAR then performs the intervention on this set of registered coordinates. A confirmation image shows a tissue sample that is removed from the previously set target in the area of enhancement, thereby indicating a successful biopsy. Although targeting error cannot be directly quantified, Figure 13 demonstrates successful targeting of a lesion and repeatability in placing all of the tools involved in a biopsy procedure. IGAR-Breast therefore achieves a clinical degree of accuracy in an end-to-end procedure.

The three broad objectives for MR compatibility are fulfilled. However, this statement is currently applicable

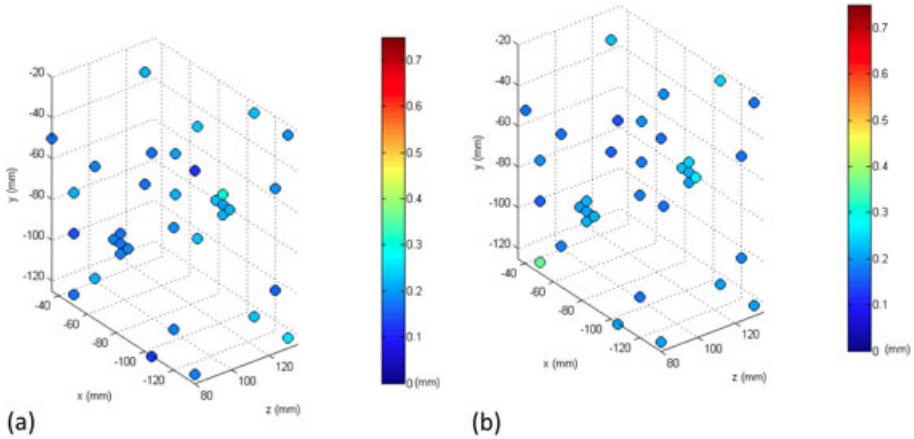

Figure 12. Repeatability for all targets in (a) IGAR 201 and (b) IGAR 202

DOI: 10.1002/rcs

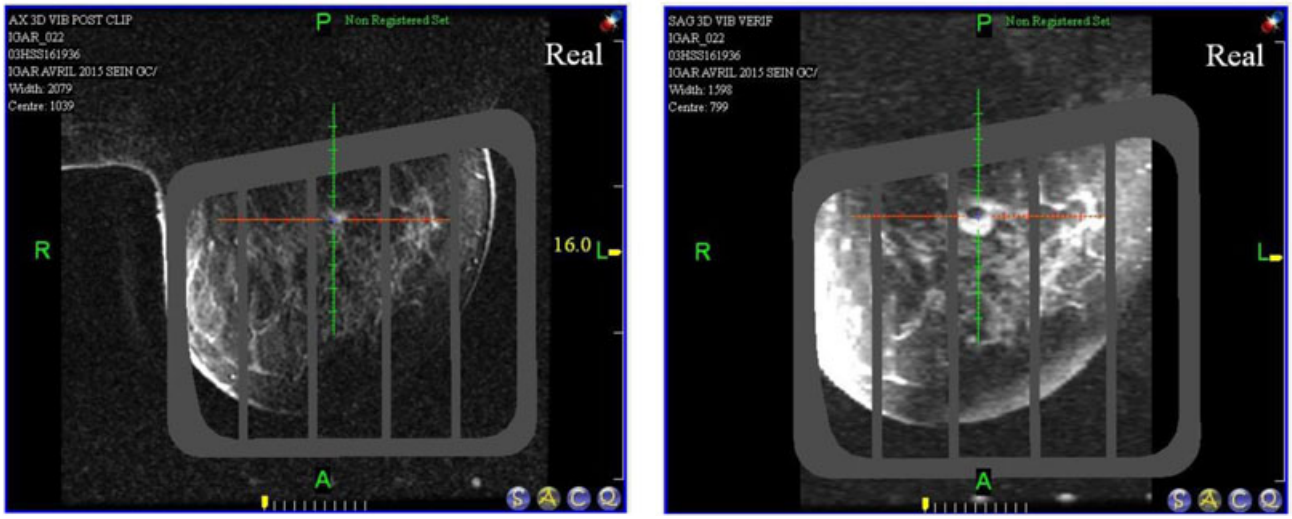

Figure 13. Left: the IGAR software interface allows a user to plan the intervention by placing a target over an enhancing lesion. Right: confirmation images show that the lesion was biopsied successfully

only in a limited sense. At most, IGAR-Breast will be loaded into the MR bore and turned on in standby mode during image sequencing. It is not within the current scope of the project to evaluate the operation of the IGAR manipulator in the isocenter of the magnet. Therefore, while the goal is to design a system functional in an MR environment, IGAR-Breast is not yet a fully MR-integrated procedure.

The ability to perform medical interventions while the patient remains in the MR scanner could reduce targeting errors attributable to patient movement while decreasing the length of the procedure. This would require an imageable biopsy tool, consequently eliminating the need for an obturator. A major roadblock to realizing this workflow is the lack of available imageable tools, as presented in Figure 4. An in-bore biopsy would require the development of new tools composed of MRI compatible cutting elements.

Mammography is the current standard imaging technique for breast cancer but it has variable sensitivity especially in dense breast. In contrast, MRI is extremely sensitive to cancer in the breast and can detect lesions that may be occult on other imaging modalities. Currently MRI is used for high risk breast cancer patients and small lesions. Those lesions detected by MRI then require MRI-guided breast biopsy, which can be difficult to perform. IGAR aims to make MRI-guided biopsy more accessible to patients and physicians, and may therefore increase the utility of and clinical indications for MRI guided biopsy.

Utilization of MRI-compatible robotic technology has several future applications to numerous patient populations. In the breast, the increased sub-millimeter accuracy combined with the high sensitivity of MRI may allow for earlier interventions on smaller lesions, potentially ones that could be fully excised on biopsy alone. This targeting ability could be leveraged for other interventional procedures including those in the brain, spine, liver, and kidney. IGAR is a platform that can perform any needle-based intervention and hold any off-the-shelf device with a simple tool adapter change. With the addition of therapy such as cryoablation IGAR could execute a 'one-stop' cancer strategy where detection, diagnosis, and intervention could be administered in a single visit.

Conclusion

Overall, test results conclude that the IGAR-Breast is suitable for operation in an MR environment. No components experience attractive forces powerful enough to induce a projectile motion and cause a safety hazard. There was no significant temperature rise on the coils or the IGAR W200 cable, and no arcing was observed. SNR results are reasonable given all the potential sources of noise inherent to the MR environment, as are distortion results. Testing configurations aimed to mimic the clinical environment in the worst-possible scenario, giving confidence that these results are reliable indications of success. Results from free space accuracy testing are encouraging and should ensure precision targeting even after additional sources of error are introduced during clinical use.

Acknowledgements

The authors would like to acknowledge the contribution of Kevin Randall, Peter Bevan, Kevin Morency, Bartholomeus Verzijlenberg and Mark Pennells during the testing conducted, and Ruth Breau and Ruwani Mahathantila for their assistance with the preparation of the manuscript

DOI: 10.1002/rcs

Conflict of interest

The authors have stated explicitly that there are no conflicts of interest in connection with this article.

Funding

No specific funding.

References

1. Ferlay J, Soerjomataram I, Ervik M, Dikshit K, Eser S, Mathers C, Rebelo M, Parkin D, Forman D, Bray F. GLOBOCAN 2012 v1.0, Cancer Incidence and Mortality Worldwide: International Agency for Research on Cancer CancerBase; 2012 [Available from: http://globocan.iarc.fr/Pages/fact_sheets_cancer.aspx.
2. de Bresser J, de Vos B, van der Ent F, Hulsewe K. Breast MRI in clinically and mammographically occult breast cancer presenting with an axillary metastasis: a systematic review. *Eur J Surg Oncol* 2010; **36**(2): 114–119.
3. Silverstein MJ, Recht A, Lagios MD, Bleiweiss IJ, Blumencranz PW, Gizienski T, Harms SE, Harness J, Jackman RJ, Klimberg VS, Kuske R, Levine GM, Linver MN, Rafferty EA, Rugo H, Schilling K, Tripathy D, Vicini FA, Whitworth PW, Willey SC. Special report: Consensus conference III. Image-detected breast cancer: state-of-the-art diagnosis and treatment. *J Am Coll Surg* 2009; **209**(4): 504–520.
4. Buchanan CL, Morris EA, Dorn PL, Borgen PI, Van Zee KJ. Utility of breast magnetic resonance imaging in patients with occult primary breast cancer. *Ann Surg Oncol* 2005; **12**(12): 1045–1053.
5. Orel SG, Weinstein SP, Schnall MD, Reynolds CA, Schuchter LM, Fraker DL, Solin LJ. Breast MR imaging in patients with axillary node metastases and unknown primary malignancy. *Radiology* 1999; **212**(2): 543–549.
6. Lehman CD, Gatsonis C, Kuhl CK, Hendrick RE, Pisano ED, Hanna L, Peacock S, Smazal SF, Maki DD, Julian TB, DePeri ER, Bluemke DA, Schnall MD, Group ATI. MRI evaluation of the contralateral breast in women with recently diagnosed breast cancer. *N Engl J Med* 2007; **356**(13): 1295–1303.
7. Warner E, Plewes DB, Shumak RS, Catzavelos GC, Di Prospero LS, Yaffe MJ, Goel V, Ramsay E, Chart PL, Cole DE, Taylor GA, Cutrara M, Samuels TH, Murphy JP, Murphy JM, Narod SA. Comparison of breast magnetic resonance imaging, mammography, and ultrasound for surveillance of women at high risk for hereditary breast cancer. *J Clin Oncol* 2001; **19**(15): 3524–3531.
8. Kuhl CK, Schmutzler RK, Leutner CC, Kempe A, Wardelmann E, Hocke A, Maringa M, Pfeifer U, Krebs D, Schild HH. Breast MR imaging screening in 192 women proved or suspected to be carriers of a breast cancer susceptibility gene: preliminary results. *Radiology* 2000; **215**(1): 267–279.
9. Morris EA, Liberman L, Ballon DJ, Robson M, Abramson AF, Heerdt A, Dershaw DD. MRI of occult breast carcinoma in a high-risk population. *AJR Am J Roentgenol* 2003; **181**(3): 619–626.
10. Stoutjesdijk MJ, Boetes C, Jager GJ, Beex L, Bult P, Hendriks JH, Laheij RJ, Massuger L, van Die LE, Wobbes T, Barentsz JO. Magnetic resonance imaging and mammography in women with a hereditary risk of breast cancer. *J Natl Cancer Inst* 2001; **93**(14): 1095–1102.
11. Lehman CD, Isaacs C, Schnall MD, Pisano ED, Ascher SM, Weatherall PT, Bluemke DA, Bowen DJ, Marcom PK, Armstrong DK, Domchek SM, Tomlinson G, Skates SJ, Gatsonis C. Cancer yield of mammography, MR, and US in high-risk women: prospective multi-institution breast cancer screening study. *Radiology* 2007; **244**(2): 381–388.
12. Mann RM, Kuhl CK, Kinkel K, Boetes C. Breast MRI: guidelines from the European Society of Breast Imaging. *Eur Radiol* 2008; **18**(7): 1307–1318.
13. Smith DN, Rosenfield Darling ML, Meyer JE, Denison CM, Rose DI, Lester S, Richardson A, Kaelin CM, Rhei E, Christian RL. The utility of ultrasonographically guided large-core needle biopsy: results from 500 consecutive breast biopsies. *J Ultrasound Med* 2001; **20**(1): 43–49.
14. Cassano E, Urban LA, Pizzamiglio M, Abbate F, Maisonneuve P, Renne G, Viale G, Bellomi M. Ultrasound-guided vacuum-assisted core breast biopsy: experience with 406 cases. *Breast Cancer Res Treat* 2007; **102**(1): 103–110.
15. ACR. American College of Radiology Practice Parameter for the Performance of Magnetic Resonance Imaging-Guided Breast Interventional Procedures, 2011.
16. Liberman L. Centennial dissertation. Percutaneous imaging-guided core breast biopsy: state of the art at the millennium. *AJR Am J Roentgenol* 2000; **174**(5): 1191–1199.
17. Lehman CD, Deperi ER, Peacock S, McDonough MD, Demartini WB, Shook J. Clinical experience with MRI-guided vacuum-assisted breast biopsy. *AJR Am J Roentgenol* 2005; **184**(6): 1782–1787.
18. Liberman L, Bracero N, Morris E, Thornton C, Dershaw DD. MRI-guided 9-gauge vacuum-assisted breast biopsy: initial clinical experience. *AJR Am J Roentgenol* 2005; **185**(1): 183–193.
19. Perlet C, Heywang-Kobrunner SH, Heinig A, Sittek H, Casselman J, Anderson I, Taourel P. Magnetic resonance-guided, vacuum-assisted breast biopsy: results from a European multicenter study of 538 lesions. *Cancer* 2006; **106**(5): 982–990.
20. Liberman L, Morris EA, Dershaw DD, Thornton CM, Van Zee KJ, Tan LK. Fast MRI-guided vacuum-assisted breast biopsy: initial experience. *AJR Am J Roentgenol* 2003; **181**(5): 1283–1293.
21. Dogan BE, Le-Petross CH, Stafford JR, Atkinson N, Whitman GJ. MRI-guided vacuum-assisted breast biopsy performed at 3 T with a 9-gauge needle: preliminary experience. *AJR Am J Roentgenol* 2012; **199**(5): W651–W653.
22. Price ER. Magnetic resonance imaging-guided biopsy of the breast: fundamentals and finer points. *Magn Reson Imaging Clin N Am* 2013; **21**(3): 571–581.
23. Chevrier MC, David J, Khoury ME, Lalonde L, Labelle M, Trop I. Breast Biopsies Under Magnetic Resonance Imaging Guidance: Challenges of an Essential but Imperfect Technique. *Curr Probl Diagn Radiol* 2016; **45**(3): 193–204.
24. Orel SG, Rosen M, Mies C, Schnall MD. MR imaging-guided 9-gauge vacuum-assisted core-needle breast biopsy: initial experience. *Radiology* 2006; **238**(1): 54–61.
25. Skandarajah AR, Mann GB. The role of magnetic resonance imaging in early breast cancer. *Asia Pac J Clin Oncol* 2012; **8**(1): 24–30.
26. Liberman L, Benton CL, Dershaw DD, Abramson AF, LaTrenta LR, Morris EA. Learning curve for stereotactic breast biopsy: how many cases are enough? *AJR Am J Roentgenol* 2001; **176**(3): 721–727.
27. Brenner RJ, Fajardo L, Fisher PR, Dershaw DD, Evans WP, Bassett L, Feig S, Mendelson E, Jackson V, Margolin FR. Percutaneous core biopsy of the breast: effect of operator experience and number of samples on diagnostic accuracy. *AJR Am J Roentgenol* 1996; **166**(2): 341–346.
28. Kuhl C. The current status of breast MR imaging. Part I. Choice of technique, image interpretation, diagnostic accuracy, and transfer to clinical practice. *Radiology* 2007; **244**(2): 356–378.
29. David J, Trop I, Lalonde L. Breast procedures guided by magnetic resonance imaging. *Can Assoc Radiol J* 2005; **56**(5): 309–318.
30. Bluvol N, Kornecki A, Shaikh A, Del Rey Fernandez D, Taves DH, Fenster A. Freehand versus guided breast biopsy: comparison of accuracy, needle motion, and biopsy time in a tissue model. *AJR Am J Roentgenol* 2009; **192**(6): 1720–1725.
31. Dogangil G, Davies BL, Rodriguez y Baena F. A review of medical robotics for minimally invasive soft tissue surgery. *Proc Inst Mech Eng H* 2010; **224**(5): 653–679.
32. Mylonas N, Damianou C. MR compatible positioning device for guiding a focused ultrasound system for the treatment of brain deseases. *Int J Med Robot* 2014; **10**(1): 1–10.

33. Yiallouras C, Mylonas N, Damianou C. MRI-compatible positioning device for guiding a focused ultrasound system for transrectal treatment of prostate cancer. *Int J Comput Assist Radiol Surg* 2014; **9**(4): 745–753.
34. Kaiser WA, Fischer H, Vagner J, Selig M. Robotic system for biopsy and therapy of breast lesions in a high-field whole-body magnetic resonance tomography unit. *Invest Radiol* 2000; **35** (8): 513–519.
35. Larson BT, Erdman AG, Tsekos NV, Yacoub E, Tsekos PV, Koutlas IG. Design of an MRI-compatible robotic stereotactic device for minimally invasive interventions in the breast. *J Biomech Eng* 2004; **126**(4): 458–465.
36. Tsekos NV, Shudy J, Yacoub E, Tsekos PV, Koutlas IG, editors. Development of a robotic device for MRI-guided interventions in the breast. Bioinformatics and Bioengineering Conference, 2001 Proceedings of the IEEE 2nd International Symposium on; 2001 4-6 Nov. 2001.
37. Kokes R, Lister K, Gullapalli R, Zhang B, MacMillan A, Richard H, Desai JP. Towards a teleoperated needle driver robot with haptic feedback for RFA of breast tumors under continuous MRI. *Med Image Anal* 2009; **13**(3): 445–455.
38. Elhawary H, Zivanovic A, Rea M, Davies B, Besant C, McRobbie D, de Souza N, Young I, Lamperth M. The feasibility of MR-image guided prostate biopsy using piezoceramic motors inside or near to the magnet isocentre. *Med Image Comput Comput Assist Interv* 2006; **9**(Pt 1): 519–526.
39. Suzuki T, Liao H, Kobayashi E, Sakuma I, editors. Ultrasonic motor driving method for EMI-free image in MR image-guided surgical robotic system. 2007 IEEE/RSJ International Conference on Intelligent Robots and Systems; 2007 Oct. 29 2007-Nov. 2 2007.
40. Morelli JN, Runge VM, Ai F, Attenberger U, Vu L, Schmeets SH, Nitz WR, Kirsch JE. An image-based approach to understanding the physics of MR artifacts. *Radiographics* 2011; **31**(3): 849–866.
41. Hargreaves BA, Worters PW, Pauly KB, Pauly JM, Koch KM, Gold GE. Metal-induced artifacts in MRI. *AJR Am J Roentgenol* 2011; **197**(3): 547–555.
42. Steckner MC, Liu B, Ying L. A new single acquisition, two-image difference method for determining MR image SNR. *Med Phys* 2009; **36**(2): 662–671.
43. Firbank MJ, Coulthard A, Harrison RM, Williams ED. A comparison of two methods for measuring the signal to noise ratio on MR images. *Phys Med Biol* 1999; **44**(12): N261–N264.

DOI: 10.1002/rcs